

BICEP3 performance overview and planned Keck Array upgrade

J. A. Grayson^{a,b}, P. A. R. Ade^c, Z. Ahmed^{b,a}, K. D. Alexander^d, M. Amiri^e, D. Barkats^d, S. J. Benton^{f,g}, C. A. Bischoff^d, J. J. Bock^{h,i}, H. Boenish^d, R. Bowens-Rubin^d, I. Buder^d, E. Bullock^j, V. Buza^{d,k}, J. Connors^d, J. P. Filippini^{h,l,m}, S. Fliescherⁿ, M. Halpern^e, S. Harrison^d, G. C. Hilton^o, V. V. Hristov^h, H. Hui^h, K. D. Irwin^{a,b,o}, J. Kang^{a,b}, K. S. Karkare^d, E. Karpel^{a,b}, S. Kefeli^h, S. A. Kernasovskiy^{a,b}, J. M. Kovac^{d,k}, C. L. Kuo^{a,b}, E. M. Leitch^p, M. Lueker^h, K. G. Megerianⁱ, V. Monticue^{a,b}, T. Namikawa^{a,b}, C. B. Netterfield^{f,q}, H. T. Nguyenⁱ, R. O'Brient^{h,i}, R. W. Ogburn IV^{a,b}, C. Pryke^{n,j}, C. D. Reintsema^o, S. Richter^d, R. Schwarzⁿ, C. Sorensen^d, C. D. Sheehy^{n,p}, Z. K. Staniszewski^{h,i}, B. Steinbach^h, G. P. Teply^{h,r}, K. L. Thompson^{a,b}, J. E. Tolan^{a,b}, C. Tucker^c, A. D. Turnerⁱ, A. G. Vieregg^{d,s,p}, A. Wandui^{a,b}, A. C. Weberⁱ, D. V. Wiebe^e, J. Willmertⁿ, W. L. K. Wu^{t,a,b}, and K. W. Yoon^{a,b}

^aDepartment of Physics, Stanford University, Stanford, CA 94305, USA

^bKavli Institute for Particle Astrophysics and Cosmology, SLAC National Accelerator Laboratory, Menlo Park, CA 94025, USA

^cSchool of Physics and Astronomy, Cardiff University, Cardiff, CF24 3AA, United Kingdom

^dHarvard-Smithsonian Center for Astrophysics, Cambridge, MA 02138, USA

^eDepartment of Physics and Astronomy, University of British Columbia, Vancouver, BC, V6T 1Z1, Canada

^fDepartment of Physics, University of Toronto, Toronto, ON, M5S 1A7, Canada

^gDepartment of Physics, Princeton University, Princeton, NJ 08544, USA

^hDepartment of Physics, California Institute of Technology, Pasadena, CA 91125, USA

ⁱJet Propulsion Laboratory, Pasadena, CA 91109, USA

^jMinnesota Institute for Astrophysics, University of Minnesota, Minneapolis, MN 55455, USA

^kDepartment of Physics, Harvard University, Cambridge, MA 02138, USA

^lDepartment of Physics, University of Illinois at Urbana-Champaign, Urbana, IL 61801, USA

^mDepartment of Astronomy, University of Illinois at Urbana-Champaign, Urbana, IL 61801, USA

ⁿSchool of Physics and Astronomy, University of Minnesota, Minneapolis, MN 55455, USA

^oNational Institute of Standards and Technology, Boulder, CO 80305, USA

^pKavli Institute for Cosmological Physics, University of Chicago, Chicago, IL 60637, USA

^qCanadian Institute for Advanced Research, Toronto, ON, M5G 1Z8, Canada

^rDepartment of Physics, University of California at San Diego, La Jolla, CA 92093, USA

^sDepartment of Physics, Enrico Fermi Institute, University of Chicago, Chicago, IL 60637, USA

^tDepartment of Physics, University of California, Berkeley, CA 94720, USA

ABSTRACT

BICEP3 is a 520 mm aperture, compact two-lens refractor designed to observe the polarization of the cosmic microwave background (CMB) at 95 GHz. Its focal plane consists of modularized tiles of antenna-coupled transition edge sensors (TESs), similar to those used in BICEP2 and the *Keck Array*. The increased per-receiver optical throughput compared to BICEP2/*Keck Array*, due to both its faster $f/1.7$ optics and the larger aperture,

Corresponding author: J. A. Grayson, jgrayson@stanford.edu

more than doubles the combined mapping speed of the BICEP/*Keck* program. The BICEP3 receiver was recently upgraded to a full complement of 20 tiles of detectors (2560 TESs) and is now beginning its second year of observation (and first science season) at the South Pole. We report on its current performance and observing plans. Given its high per-receiver throughput while maintaining the advantages of a compact design, BICEP3-class receivers are ideally suited as building blocks for a 3rd-generation CMB experiment, consisting of multiple receivers spanning 35 GHz to 270 GHz with total detector count in the tens of thousands. We present plans for such an array, the new “BICEP Array” that will replace the *Keck Array* at the South Pole, including design optimization, frequency coverage, and deployment/observing strategies.

Keywords: Cosmic Microwave Background, Inflation, Gravitational Waves, Polarization, BICEP, Keck Array

1. INTRODUCTION

The precise measurement of the polarization of the Cosmic Microwave Background (CMB) is an active area of experimental physics, motivating a variety of current and upcoming polarimeter projects. The CMB temperature anisotropy, measured to extreme precision over the last two decades, has provided evidence for the standard model of Big Bang cosmology and hints at an inflationary period. In the same way, the CMB polarization, and in particular the curl ‘B-mode’ pattern, contains a wealth of cosmological information on many scales and continues to be targeted by experimentalists. At arcminute scales on the sky, the dominant B-mode signal is primarily due to the gravitational lensing of the much brighter, curl-free ‘E-mode’ signal. This lensing B-mode signal probes the large scale structure of the universe that sits between the CMB surface and ourselves and has recently been detected by POLARBEAR,¹ SPTpol,² and BICEP2/*Keck Array*.^{3,4}

At larger, degree-scales on the sky, the B-mode signal due to inflationary gravitational waves (IGW) is predicted to peak with an as-yet-unmeasured amplitude. During inflation, quantum fluctuations are expected to produce both density and gravitational wave perturbations, the latter of which imprints a B-mode pattern on the CMB. The ratio of the amplitude of the primordial tensor spectrum to the scalar spectrum, parametrized as r , is a measurable quantity that will constrain inflationary models. To this end, experiments aim to continually lower the upper-limit on, and eventually detect, the IGW B-mode signal and the resulting r parameter, a recent summary of which is given in Ref. 5.

The BICEP/*Keck* series of South Pole-based CMB polarimeters has focused efforts on this IGW B-mode signal, taking the unique approach of using compact, refracting telescope receivers that only resolve the larger degree-scale features necessary. This approach precludes science at the smaller scales but has several advantages for IGW signal sensitivity. The first experiment, BICEP1, observed for three seasons from 2006–2008 using 98 feedhorn-coupled bolometers (split primarily between 100 and 150 GHz band centers) and found a 95% confidence upper limit of $r < 0.70$.⁶ BICEP2 followed with three observing seasons from 2010–2012, using 500 antenna-coupled transition edge sensor (TES) bolometers centered at 150 GHz. It detected on-sky B-mode signal, later found to be consistent with galactic dust foregrounds, for a combined limit $r < 0.12$ at 95% confidence with *Keck Array* and *Planck* data.^{3,7} While BICEP2 was still operating, *Keck Array* began observing on a nearby telescope mount, with first science observations in 2012. *Keck Array* is made up of 5 BICEP2-class receivers sharing a common boresight. It is currently in its fifth observing season and has now included receivers centered on multiple frequencies (95, 150, and 220 GHz) in order to help distinguish polarized galactic foregrounds from the IGW signal. The latest results give $r < 0.09$ at 95% confidence,⁴ or $r < 0.07$ when combined with external datasets.

BICEP3 replaces BICEP2 and is now in its second observing season (and first science season) during the 2016 austral winter, with a full complement of 2560 TES bolometers at 95 GHz. With its larger aperture, faster optics, and higher detector count, BICEP3 acts as a pathfinder receiver for the 3rd-generation of the BICEP/*Keck* series. Its relatively compact design with on-axis optics again lends itself to multi-frequency observations, in the same way that BICEP2 was evolved into the *Keck Array*. Such an expansion to an array is highly motivated by the continued need for increasing observation depth combined with discrimination of galactic foregrounds, and is easily realized by upgrading the *Keck Array* with BICEP3-class receivers.

In the following sections, these proceedings first give an overview of the BICEP3 instrument (Sec. 2) and its South Pole observing location and strategy (Sec. 3). It then summarizes BICEP3’s current, second-season status and performance (Sec. 4) before finally outlining plans for a future multi-frequency array of BICEP3-class receivers (Sec. 5).

2. INSTRUMENT OVERVIEW

Like its BICEP/*Keck* predecessors described in Sec. 1, BICEP3 is composed of a single cryostat, also called the receiver, which contains all of the detectors and optical components required for its measurement of the CMB. This compact design, which keeps all optics at cryogenic temperatures, maintains the practical and scientific advantages of the previous BICEP/*Keck* experiments. Namely,

- the cryostat lends itself to complete assembly and disassembly by a small crew of experienced people;

- the compact, on-axis optics allow for symmetric rotation of the telescope as a whole, an important method for probing systematics in the polarization-based measurement;
- the compact optics allow for ground-based characterization in the optical far-field;
- the compact receiver size allows installation of a comoving absorptive forebaffle that terminates beam sidelobes and reduces stray pickup;
- and the ability to cryogenically cool the optical elements and internal baffling minimizes the thermal photon noise seen by the detectors and leads to excellent stability.

This section provides a short overview of the BICEP3 instrument in its current, 2016 observing season state, offered here as both a recap before giving a status update in Sec. 4, and to highlight features that will transfer over to a future BICEP3-class array as outlined in Sec. 5. A more detailed overview before the first (2015) season deployment is found in Ref. 8, and an in-depth design and operation summary during the 2015 season is provided in Ref. 9.

2.1 Cryostat Receiver

The BICEP3 receiver is a custom aluminum dry cryostat, 2.4 m tall along the optical axis with a 0.73 m outer diameter and totalling roughly 550 kg without attached readout electronics and forebaffle. Fig. 1 shows a cutaway view of the BICEP3 CAD model in this state. The top of the receiver is capped by a 31.75 mm thick high-density polyethylene (HDPE) window through which light is collected, while the bottom end is used to interface to electronic subsystems. From the side protrudes a vacuum shell extension that houses the single PT415* two-stage pulsetube cryocooler, which provides continuous cooling to <4 K.

The cryogenic design can be simply described as concentric cylindrical aluminum shells, each an increasingly cold and thermally isolating radiation shield that together protect the sub-Kelvin detectors from warm radiation. Moving inward from the room-temperature vacuum shell are the nominal ‘50 K’ and ‘4 K’ stages, respectively cooled by the 1st and 2nd stages of the pulsetube. The pulsetube is thermally linked to the 50 K and 4 K stages in the main body of the cryostat via oxygen-free high-conductivity (OFHC) copper heat straps, including flexible foil and braid sections to minimize transmission of vibrational energy from the pulsetube. Within the 4 K shield is a series of stacked planar ‘sub-Kelvin’ stages (2 K, 350 mK, 250 mK) culminating in the 250 mK focal plane (Fig. 2). The various temperature stages are structurally supported and thermally isolated from each other by trusses of low thermal-conductivity materials (G10 fiberglass and carbon fiber).

A three-stage ($^4\text{He}/^3\text{He}/^3\text{He}$) helium sorption fridge[†] is mounted on the 4 K stage near the pulsetube and provides non-continuous cooling for all three sub-Kelvin stages. The three stages of the fridge contain 55 L of ^4He and 33 L/4 L of ^3He at standard temperature and pressure, able to cool BICEP3’s detector modules and large copper focal plane from 4 K to 250 mK and then maintain operating temperatures for more than 48 hours before needing to re-cycle.

The 250 mK stage is separated into two planar copper stages to provide thermal stability for the detectors. The lower level, closest to the 350 mK stage, is actively temperature-controlled to 269 mK by a resistive heater and acts as a buffer for the more isolated focal plane. Stainless steel blocks separate the two levels and provide low-pass thermal filtering. The focal plane itself is additionally temperature-controlled to 274 mK.

2.2 Detectors and Readout

BICEP3’s focal plane is populated by planar arrays of polarization-sensitive slotted antennas, coupled to transition edge sensor (TES) bolometers and centered at 95 GHz, the same technology also fabricated by JPL/Caltech for BICEP2/*Keck Array* and detailed in Ref. 10. Each silicon detector tile contains an 8×8 array of pixels with each pixel made up of two co-located, orthogonally-polarized sub-antenna networks and two TES bolometers. A Gaussian taper of each pixel’s beam is achieved by tuning the summing tree that couples each bolometer to its

*Cryomech Inc., Syracuse, NY 13211, USA (www.cryomech.com)

†Chase Research Cryogenics Ltd., Sheffield, S10 5DL, UK (www.chasecryogenics.com)

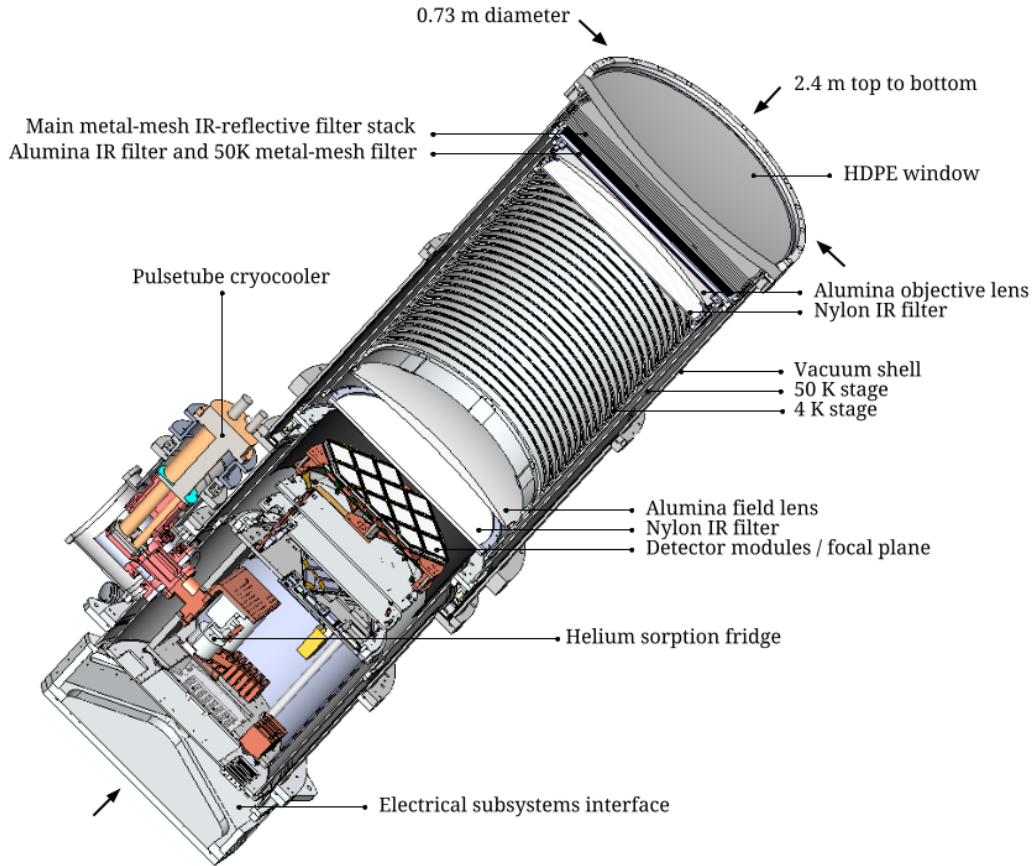


Figure 1: Cutaway view of the BICEP3 cryostat receiver, with key elements labeled.

sub-antenna network.¹¹ A major difference from BICEP2/*Keck Array* is the installation method of detector tiles on the focal plane. In BICEP2/*Keck* receivers, four detector tiles are directly wire bonded to the focal plane, and the supporting readout electronics sit adjacent at the focal plane’s outer radius. BICEP3 instead packages each detector tile and its electronics in a more easily installed compact detector module. The concurrently presented Ref. 12 describes these detector modules in more detail.

Twenty such detector modules are tiled onto the BICEP3 focal plane, each containing 128 TES bolometers, for a total of 2560. Each detector tile contains 8 ‘dark’ TES bolometers that are intentionally left uncoupled to antennas, 4 of which are read out as non-optical probes, giving a total of 2400 optically-coupled bolometers or, equivalently, 1200 polarization-sensitive detector pairs centered at 95 GHz. This contrasts to a single BICEP2/*Keck Array* receiver at 150 GHz, which has four detector tiles for a total of 248 polarization-sensitive detector pairs. At 95 GHz, a single *Keck Array* receiver provides an even sharper comparison with 136 polarization-sensitive detector pairs, owing to its slower optics and smaller aperture than BICEP3.

BICEP3 continues to use time-domain multiplexed (TDM) readout of the TES bolometers, via SQUID MUX chips developed by NIST, in order to reduce the total number of lines that must enter the cryostat and their associated heat load. The signal current through each voltage-biased TES is inductively coupled to its own 1st-stage SQUID series array, forming one column of one multiplexed ‘row’. A pair of 11-row MUX chips is wire bonded in series in order to allow multiplexing through 22 rows. Each detector module contains 6 pairs of MUX chips, forming 6 columns of 22 rows, or 132 total 1st-stage channels. Each column’s multiplexed output is inductively coupled to a separate SQUID series array on the 4 K stage for additional amplification before exiting the cryostat. BICEP3 uses MUX11d chips, a newer generation than those used by BICEP2/*Keck Array*¹³ that has a different row-switching mechanism. Details of the new design are found in the concurrently presented

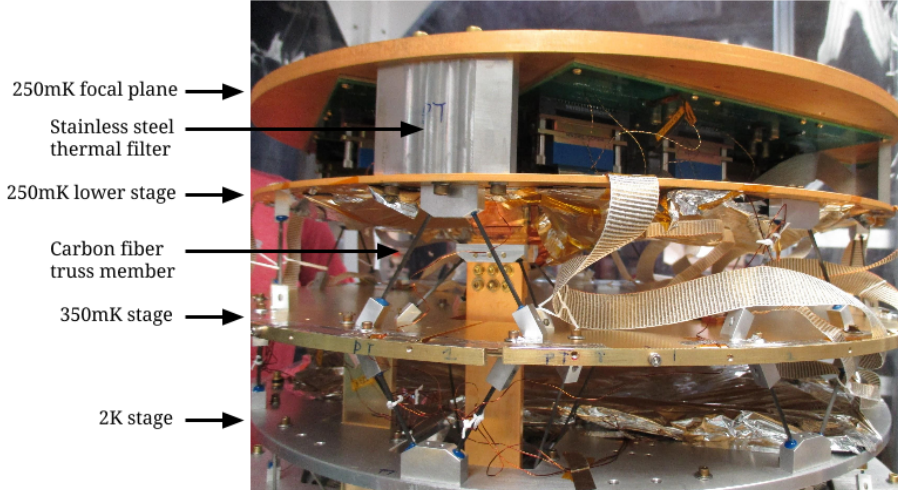


Figure 2: The BICEP3 sub-Kelvin stages exposed during assembly, with various components labeled.

Ref. 12. Control of the MUX system and feedback-based readout of the TES data are via room temperature Multi-Channel Electronics (MCE) systems developed by the University of British Columbia,¹⁴ again similar to those used in BICEP2/*Keck Array*.

2.3 Optics and IR Filtering

Following the other BICEP/*Keck* experiments, BICEP3 targets degree-scale polarization features by using a compact, on-axis, two-refractor optical design. Its $f/1.7$ system with a 27.4° field of view (FOV) is faster and wider than the $f/2.2$, $\text{FOV} \sim 15^\circ$ optics of BICEP2/*Keck Array*. It has a significantly larger aperture diameter of 520 mm, vs. 264 mm for BICEP2/*Keck Array*, defined by a millimeter-wave absorbing aperture stop. Both refracting lenses and the aperture stop are heatsunk to the 4 K stage, with the objective lens (warmest and furthest from the focal plane) operating at 4.9 K. The lenses are made of 99.6% pure alumina ceramic, which allows a thinner design and smaller thermal gradients than the HDPE plastic used for previous BICEP/*Keck* optics, crucial advantages for BICEP3's faster system and increased infrared (IR) thermal loading.

The much larger diameter of the BICEP3 receiver window (~ 670 mm clear), necessitated by the increase in aperture size, creates a large IR radiative heat load. IR power entering the cryostat is in excess of 100 W, more than $2\times$ the cooling power of the 1st stage of the single PT415 pulsetube cooler. The first level of IR filtering therefore attempts to reject the majority of IR loading before it reaches the 50 K stage, and consists of a stack of 10 metal-mesh IR-reflective filters mounted just within the receiver window at room temperature. These filters are made up of $\mathcal{O}(10 \mu\text{m})$ capacitive squares created by laser ablation of aluminized thin plastic films ($3.5 \mu\text{m}$ Mylar or $6 \mu\text{m}$ polypropylene (PP)/polyethylene (PE) blend), as introduced in Ref. 15. In all, through both reflection and absorption/reemission, the metal-mesh filter stack allows ~ 19 W to reach the 50 K stage. One additional metal-mesh filter is mounted just behind the 50 K alumina filter. The remaining power is absorbed by a series of three filters (and thereby removed by the pulsetube) in order to shield the sub-Kelvin detector stage: a 10 mm thick alumina filter on the 50 K stage, between the metal-mesh filter stack and the objective lens; a 5 mm thick nylon filter on the 4 K stage, between the two lenses; and a second 4 K nylon filter, 9.5 mm thick, between the field lens and the focal plane. These IR filters and lenses are labeled in Fig. 1. Finally, low-pass metal-mesh edge filters¹⁶ with a 4 cm^{-1} (120 GHz) cutoff are mounted onto each detector module to prevent any remaining out-of-band sub-millimeter blue leaks from coupling to the detector bolometers.

3. OBSERVING SITE AND STRATEGY

The BICEP3 receiver is integrated with its telescope mount and various subsystems in the Dark Sector Laboratory (DSL) building at the South Pole, from where it observes the sky during the austral winter. Support and logistics



Figure 3: View of BICEP3 from the roof of DSL, showing the green insulating boot, comoving forebaffle, and reflective ground shield. The larger *Keck Array* ground shield is visible in the background and the main Amundsen-Scott station extends along the horizon.

are managed through the US National Science Foundation’s Amundsen-Scott South Pole Station, located 1 km away, including satellite-based daily transfer of the full science data stream. This cold and remote observing site sits at an elevation of over 2800 m on the Antarctic Plateau and provides extremely dry and stable atmospheric conditions, optimal for BICEP3’s millimeter-wave observations.

The warmed indoor environment of DSL is extended beyond the roof level by a flexible insulating boot so that only the receiver window is exposed to the outdoor environment (Fig. 3). A dry nitrogen gas system fills a protective membrane above the receiver window to prevent snow accumulation, and a cylindrical comoving microwave-absorptive forebaffle extends beyond the receiver window to intercept stray light. A reflective, stationary ground shield is fixed to the roof of DSL and acts as a second barrier against signal contamination from nearby ground sources.

BICEP3 continues to use the original three-axis BICEP1 mount in DSL that also supported BICEP2. By removing some non-essential structures, the mount was modified to fit BICEP3’s larger size while retaining the same functions: ranges of $>360^\circ$ in azimuth, 50° – 90° (zenith) in elevation, and boresight rotation about the optical axis (Fig. 4). Due to the larger diameter of BICEP3 and the protruding vacuum shell extension that houses the pulsetube cooler, boresight rotation is limited by mechanical interference to a range of 255° . All electrical cabling, high-pressure helium gas hoses for the pulsetube, and other necessary lines are routed through cable carriers for the three axes of motion, with the exception of a 4-channel high-pressure rotary joint[‡] used to bypass the two helium hoses at the azimuth stage. By pressurizing two outer channels to act as buffers to atmosphere, the 4-channel rotary joint achieves much better leak performance than the 2-channel unit used during BICEP3’s 2015 season; the optimal pulsetube system pressure is maintained by small, non-disruptive refills to the compressor less than once a month.

BICEP3 focuses its CMB observations on the same sky patch as the *Keck Array* and previous BICEP experiments, spanning right ascension $-60^\circ < RA < 60^\circ$ and declination $-70^\circ < \delta < -40^\circ$. Its larger optical FOV results in an effective sky area of $\sim 600 \text{ deg}^2$, larger than the $\sim 400 \text{ deg}^2$ area covered by BICEP2/*Keck*. The fundamental observing block is a constant-elevation ‘scanset’ of 50 back-and-forth 2.8 deg/s fixed-center azimuth scans spanning 64.4° . Each scanset is bookended by a 26 s elevation nod of 1.3° peak to peak for airmass-based detector gain calibration and ~ 1 minute of partial TES loadcurves (non-superconducting) to monitor detector

[‡]Dynamic Sealing Technologies, Inc., Andover, MN 55304, USA (www.dsti.com)

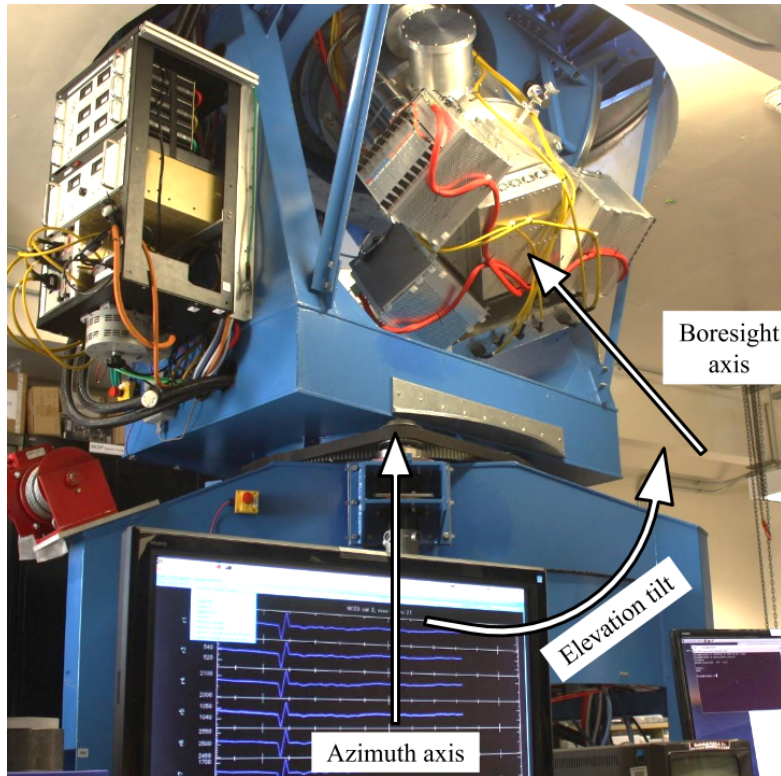


Figure 4: BICEP3 observing on the original BICEP mount, with the three axes of motion labeled.

parameters, for a total duration of ~ 50 minutes. The azimuth center is adjusted every other scanset to track the changing RA of the sky patch, using that drift in combination with the field of view to fill in the full range in RA. Elevation is staggered by twenty 0.25° offsets amongst the scansets to fill in coverage of the detector beam pattern.

Observations are on a two-sidereal day cadence, including 40 CMB scansets and 7 scansets aimed at the galactic plane. Each two-day cycle uses one of four boresight angles within the allowed boresight envelope to help constrain polarization systematics: two sets of 180° opposing orientations, offset from each other by 45° , and clocked to optimize coverage symmetry of both the Stokes Q and U polarizations on the sky. The first 6.5 hrs of each cycle is spent re-cycling the helium sorption fridge to keep the detectors cold for the rest of the two days.

4. CURRENT PERFORMANCE

BICEP3's first season performance, during the 2015 austral winter, is summarized in Ref. 17. During that initial engineering season, 9 of the possible 20 detector modules were installed, for a total of 540 polarization-sensitive detector pairs centered at 95 GHz. Yield after accounting for known hardware issues (e.g. suspected broken wire bonds, SQUID MUX chip yield) was 436 good polarization-sensitive pairs, or 81%. 51 of the 104 lost pairs were attributed to a single anomalously low-yield detector module, potentially due to wire bond or other damage to the detector tile during installation and receiver cool-down. Median per-detector CMB noise-equivalent temperature (NET) for the 2015 season is estimated at $449 \mu\text{K}\sqrt{\text{s}}$, based on polarization pair-differenced timestream data as shown in Fig. 5 and explained later in this section.

BICEP3 underwent a number of improvements during the 2015/16 austral summer in preparation for its second season in the 2016 austral winter, which is the first dedicated science season. As originally planned, the focal plane was populated with the full complement of 20 detector modules, including 12 new detector modules

and the removal of the anomalously low-yield module mentioned above. Additionally, several important changes were made in response to data and operations knowledge collected during the 2015 season.

First, cryogenic improvements have added over 20% to the helium sorption fridge duty cycle and allow the current two-day observing schedule cadence. During the 2015 season, continuous observing time was limited by the fridge to 12 hrs. This cryogenic fix came in two parts, both vetted by parallel lab testing in North America during BICEP3's 2015 season observations. Lowering of the helium sorption fridge bath temperature by 0.6 K, to 3.5 K, was achieved by increasing thermal conduction through the copper heatstrap to the pulsetube's 2nd stage and thereby allowed increased helium condensation during the fridge re-cycling. Furthermore, a foil shielding included on a small number of electrical cables was measured to give an excess 200 μ W parasitic conductive heat load to the nominal 350 mK stage, at least tripling the total expected load. Removal of this incorrectly specified shielding resulted in a large 280 mK reduction on that stage, allowing it to reach 360 mK, which in turn allowed lowering the focal plane operating temperature from 313 mK to 274 mK for the 2016 season.

Second, two faulty metal-mesh IR-reflective filters were replaced for 2016 and have significantly reduced broad and polarization-dependent scattering of the 95 GHz signal. This has been measured both as a per-detector 26% median reduction of loading from the comoving forebaffle, and as an improvement in detector loading median mismatch from $\sim 10\%$ to $< 3\%$ between co-located orthogonally polarized detectors when observing broad sources (forebaffle and atmosphere). Lab inspection has shown these faulty filters to be plagued by incomplete and inconsistent laser ablation of the aluminization on micron scales, now easily remedied with replacements and improved screening.

Finally, 2015 season data showed BICEP3 to be sensitive to 450 MHz interference from the main South Pole Station radio system, owing to its larger receiver aperture than BICEP2/*Keck Array* (Sec. 2.3) and correspondingly lower high-pass waveguide cutoff frequency. The interference caused a mostly ground-fixed signal, but also contributed to transients in the feedback-based detector readout. For the 2016 season, internal RF shielding improvements at the focal plane have given a ~ 10 dB reduction in RF signal sensitivity, and changes at the main station (reduced output power and a directional antenna) have reduced the signal strength at DSL by ~ 35 dB, for a total ~ 45 dB reduction.

As is routine for the BICEP/*Keck* experiments, BICEP3 was subject to several calibration measurements during the 2015/16 austral summer in order to characterize the instrument before the 2016 observation season. Per-detector spectra were measured for all 20 modules with a custom Martin-Puplett Fourier Transform Spectrometer (FTS)¹⁸ mounted to the window of BICEP3 while in the mount. Optical efficiency through the receiver was measured with an aperture-filling liquid nitrogen load mounted above the receiver window, which also acted as an ambient temperature source when unfilled. Results from both measurements can be found in the concurrently presented Ref. 12. Far-field beam characteristics were measured over several weeks using a chopped thermal source mounted high above the nearby Martin A. Pomerantz Observatory building (the location of *Keck Array*) and are covered in detail in the concurrently presented Ref. 19.

As of writing in early June 2016, BICEP3 has observed for ~ 2.5 months in its second season and accumulated roughly 1224 receiver-hours of new CMB data. Overall detector yield due to known hardware issues is 951 good polarization-sensitive pairs, or 79%. 180 of the 249 lost pairs are due to electrical open circuits that developed on 7 SQUID MUX row-select lines shared by a group of 5 detector modules. The cause of the bad connections is yet to be determined and only became present after cryogenic cooling of the receiver. Because these row-select lines are run in series, it is possible that poor wire bond adhesion within a single detector module could be the culprit. The number of lost detector pairs is magnified due to polarization pairing across adjacent MUX rows (pairs are wired along the same MUX column, rather than row, sharing common parameters such as SQUID and TES biases).

The median noise spectrum and per-detector, per-scanset noise distribution is shown in Fig. 5, based on the timestreams for all CMB data so far during the 2016 season. The timestream data has been differenced between polarization pairs, with basic cuts applied so that only good pairs remain (based on both the known hardware yield and preliminary data-quality cuts). Pair-summed spectra are also shown to demonstrate the $1/f$ noise rejection of the pair-difference polarization data. Conversion to CMB temperature is done by calibration of a BICEP3 CMB temperature map to 100 GHz Planck data. The histogram shows science-band average noise after

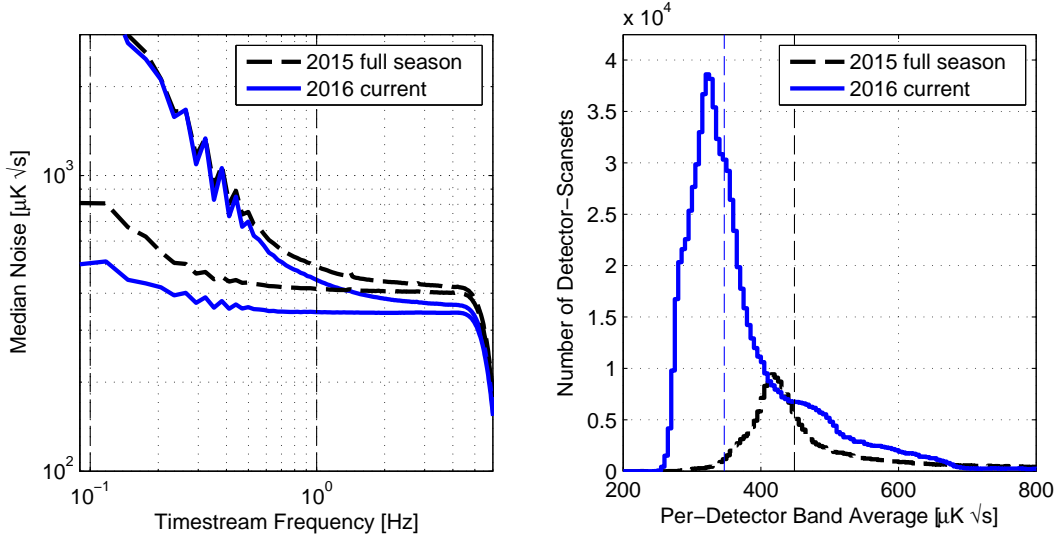


Figure 5: *Left*: Median per-detector noise spectra for BICEP3 2015 and 2016 season data, from both pair-summed and pair-differenced minimally processed timestreams (showing $1/f$ noise rejection of the differenced polarization measurement). *Right*: Histogram of the per-detector per-scanset noise, applying 3rd-order polynomial timestream filtering and averaged across the 0.1-1 Hz science band. Median values of $449 \mu\text{K}\sqrt{\text{s}}$ and $347 \mu\text{K}\sqrt{\text{s}}$ are marked by vertical dashed lines for the 2015 and 2016 data, respectively. Significantly increased detector population and observing duty cycle explain the much larger 2016 histogram amplitude, which will continue to grow as the season progresses.

filtering the timestreams with a 3rd-order polynomial during every unidirectional azimuth scanning movement (100 moves per scanset) to mimic final map making. BICEP3’s 2015 season data is also shown for comparison.

An improvement in per-detector sensitivity is clear, summarized by the improved per-detector median band-average NET of $347 \mu\text{K}\sqrt{\text{s}}$ for the 2016 season versus $449 \mu\text{K}\sqrt{\text{s}}$ from the 2015 season data (right panel of Fig. 5). However, *Keck Array* 95 GHz data shows a median $280 \mu\text{K}\sqrt{\text{s}}$ with the same treatment. Reduction of scattering and the resulting detector photon load from warm surfaces, along with the reduction of RF interference, both detailed earlier in this section, can explain BICEP3’s improvement in the 2016 season, but a detailed quantification and an understanding of the performance relative to *Keck Array* detectors is ongoing. Combining the band-average NET values across all detectors for each scanset gives a BICEP3 2016 median array NET of $9.91 \mu\text{K}\sqrt{\text{s}}$. This value accounts for hardware yield (79%) and for preliminary data-quality cuts (currently a $\sim 45\%$ loss). BICEP3 2015 data gives a much higher median array NET of $24.6 \mu\text{K}\sqrt{\text{s}}$ due to the higher per-detector NET, the only partially populated focal plane, and a higher ($\sim 58\%$) loss to data-quality cuts.

All above quoted NET values in this section are based on timestream data. This is an important distinction and the values are not meant to be directly comparable to map-based NET estimates. Specifically, Ref. 17 and Ref. 12 quote map-based BICEP3 per-detector NET estimates of $395 \mu\text{K}\sqrt{\text{s}}$ (2015 season) and $333 \mu\text{K}\sqrt{\text{s}}$ (2016 season). The difference arises from details of the two NET estimations. The map-based value is an estimate based on the standard deviation across all map pixels of a polarization noise map, accounting for the weighted integration time of each pixel, and is therefore insensitive to details of individual detector spectra and assumes a Gaussian noise distribution that will not necessarily reproduce a median of the distributions shown in Fig. 5. Additionally, the timestream-based value averages across 0.1–1 Hz, not the full range of scales considered in the map-based method described. The two methods converge more closely for the total BICEP3 array NET, for which the map-based method gives $9.72 \mu\text{K}\sqrt{\text{s}}$.¹²

5. FUTURE MULTI-RECEIVER ARRAY

Plans have begun to upgrade the *Keck Array* to a 3rd-generation, or “Stage 3”, experiment with BICEP3-class receivers. The *Keck Array*, the culmination of the BICEP2/*Keck* 2nd-generation, demonstrates the scalability of BICEP2-class receiver technology and the efficiency of frequency expansion through an array model in which the optics and detectors of each receiver can be tuned to a single frequency band. For the 2014 observing season, two of the five 150 GHz *Keck Array* receivers were replaced with 95 GHz detectors and matching optics. That additional data allowed a more extensive model of the polarized galactic foreground, and for the first time showed B-mode constraints to be the most powerful on the IGW signal (beyond constraints derived from CMB temperature and other evidence).⁴ In the following 2015 observing season, two more 150 GHz *Keck Array* receivers were refitted, this time with 220 GHz detectors and optics, further broadening the spectral coverage of the combined data set by reaching to the higher-frequency polarized dust signal. Most recently, now that BICEP3 is fully populated at 95 GHz for the current 2016 observing season, the two 95 GHz *Keck Array* receivers were also refitted to 220 GHz, for a total of four at 220 GHz.

With its $5\times$ higher per-receiver detector count, the BICEP3 design acts as a building block for this 3rd-generation multi-frequency CMB polarimeter that we have chosen to name BICEP Array. In order to continue to further constrain the IGW signal and aim for primordial B-mode detection, BICEP Array will focus its increased total detector count ($\sim 12\times$ greater than *Keck Array*) on the same sky patch from the South Pole. This shared sky patch with all other BICEP/*Keck* experiments covers $\sim 1\%$ of the sky, sufficient area to search for the degree-scale (multipole $l = 80$) recombination bump B-mode signal. With the large amount of accumulated observations, it remains the preferred patch to continue with deeper, multi-frequency observations for targeted degree-scale IGW signal detection and improved galactic foreground separation.

BICEP Array will be 4 new BICEP3-class receivers with frequency band centers spanning 35 to 270 GHz. The design of a BICEP3-class receiver was detailed in Sec. 2, showing how BICEP3 expanded to higher detector count and larger aperture while maintaining the advantages of the compact, on-axis, cold refractor design shared by the BICEP/*Keck* program. A number of changes are expected to improve on the BICEP3 design. Testing of the metal-mesh IR-reflective filter design has been ongoing since its first development for BICEP3, and potential changes include double-sided aluminization and laser patterning so that fewer filters are required to achieve the same IR rejection. Heatsinking the metal-mesh filter stack to 50 K, rather than the room temperature vacuum shell as in BICEP3, could also reduce IR loading from the emissive substrate films.

Some changes are also expected for the detector modules used in BICEP Array. The four receivers will separately have focal planes centered on 35, 95, and 150 GHz, and lastly a 220/270 GHz hybrid. Each focal plane will be made up of BICEP3-style detector module packages but will use 6” rather than 4” silicon wafer processes and require many fewer than 20 modules to fill the focal plane, thereby reclaiming focal plane area lost to the module borders. Table 1 shows the nominal number of detectors that will fit into each focal plane of BICEP Array. The 220/270 GHz dust-control receiver will have detectors at the two frequencies in a checkerboard array on the focal plane, based on the current 220 GHz *Keck Array* detectors and a lab-tested 270 GHz design that will be introduced into *Keck Array* for the 2017 season. The extremely high 220/270 GHz detector count motivates frequency domain multiplexing readout schemes as a possible alternative to BICEP3’s SQUID-based TDM readout (which will continue to be used for the lower frequency receivers). The 35 GHz receiver will help constrain galactic synchrotron emission at the level required for BICEP Array’s sensitivity; prototyping and testing of the 35 GHz detectors is currently underway. Fig. 6 shows a comparison of the proposed BICEP Array design to its predecessors, including the focal plane size and frequency mix.

BICEP Array will use a new mount at the South Pole to hold all 4 BICEP3-class receivers, each arranged around a common boresight, as the increased receiver size cannot be accommodated by the existing *Keck Array* mount (originally built for the DASI experiment). The use of high-pressure helium rotary joints, operating successfully with BICEP3, will help reduce the total size of the new mount by avoiding a significant volume of helium hose in the azimuth and theta stages. BICEP Array will replace the *Keck Array* and observe simultaneously with the ongoing BICEP3 program. The 35 GHz receiver is under development and is planned to be the first of the BICEP Array, beginning as early as the 2018 observing season. Three *Keck Array* receivers outfitted at 270 GHz will fill the remaining spots of the new mount. Before the second observing season, the 95 and 150 GHz receivers

Experiment	Frequency Band (GHz)	TES Detector Count Per Receiver	Survey Weight Per Year Per Receiver ($\mu\text{K}^{-2} \text{ yr}^{-1}$)
<i>Keck Array</i>	95	288	24000
	150	512	30000
	220	512	2000
	270	512	800
BICEP3	95	2560	213000 [§]
BICEP Array	35	384	37000
	95	3456	287000
	150	7776	453000
	220	9408	37000
	270	9408	15000

Table 1: Nominal number of TES detectors and survey weight per year for each of the four BICEP Array receivers (220 GHz and 270 GHz make up one receiver), and a comparison to BICEP3 and *Keck Array*. Bolded detector counts are from fielded receivers. Maximum *Keck Array* (BICEP Array) population across 5 (4) receivers is 2560 (30432) detectors. Bolded survey weights are achieved results, indicating performance taking into account all real world observing inefficiencies (see text for details). Other survey weights are scaled from the bolded values.

will be installed, and finally the 220/270 GHz receiver will complete the array for the third and subsequent observing seasons.

A useful metric to quantify the CMB polarization sensitivity and the statistical sensitivity to r that will be achieved with BICEP Array is the survey weight $W = 2A/N^2$ (units of μK^{-2}), where A is the map area and N is the polarization map depth (e.g. units of $\mu\text{K}\cdot\text{degrees}$). Conveniently, survey weight scales linearly with detector count and integration time, and Table 1 shows a comparison of survey weights per year for *Keck Array* and BICEP Array receivers. The *Keck Array* 95 GHz survey weight is based on the 2014 season published result,⁴ while the 150 GHz survey weight is based on both BICEP2 performance³ and the latest published 3 receiver-years of *Keck Array*.⁴ The *Keck Array* 220 GHz survey weight is based on preliminary results from the first season (2015) of receivers at that frequency. These achieved values are then simply scaled by the squared ratio of nominal per-detector NET values (taking into account e.g. detector parameters, loading from optical elements and the atmosphere) to 35 and 270 GHz, and the BICEP Array values are further scaled by the ratio of detector counts. In this way, all values take into account all real world observing inefficiencies of the BICEP2/*Keck* experiments. From this treatment it is clear that the BICEP Array represents an order of magnitude upgrade in total raw experimental sensitivity versus *Keck Array*.

6. CONCLUSION

These proceedings have summarized the instrument design and observation strategy of the BICEP3 polarimeter, and reported on changes and current performance for its ongoing second season. Important changes included full detector population of the focal plane, cryogenic improvements that led to increased observation duty cycle, replacement of under-performing IR filters, and a significant reduction in RF interference. Based on the first ~ 1224 hours of new CMB data this season (2016), BICEP3 has a timestream-based median per-detector NET of $347 \mu\text{K}\sqrt{\text{s}}$ and an array NET of $9.91 \mu\text{K}\sqrt{\text{s}}$ for the whole instrument, an improvement over the 2015 per-detector median of $449 \mu\text{K}\sqrt{\text{s}}$.

Plans were also outlined for an upgrade to the multi-frequency *Keck Array*, named BICEP Array. BICEP Array will be four BICEP3-class receivers spanning 35 to 270 GHz and begin a staggered deployment as soon as 2018.

[§] The quoted BICEP3 survey weight is scaled from the *Keck Array* 95 GHz value, reflecting the eventual expectation for BICEP3. Adjusting by the BICEP3 and *Keck Array* median per-detector band average NET values quoted in Sec. 4 gives an estimated BICEP3 survey weight of $139\,000 \mu\text{K}^{-2}$ for 2016.

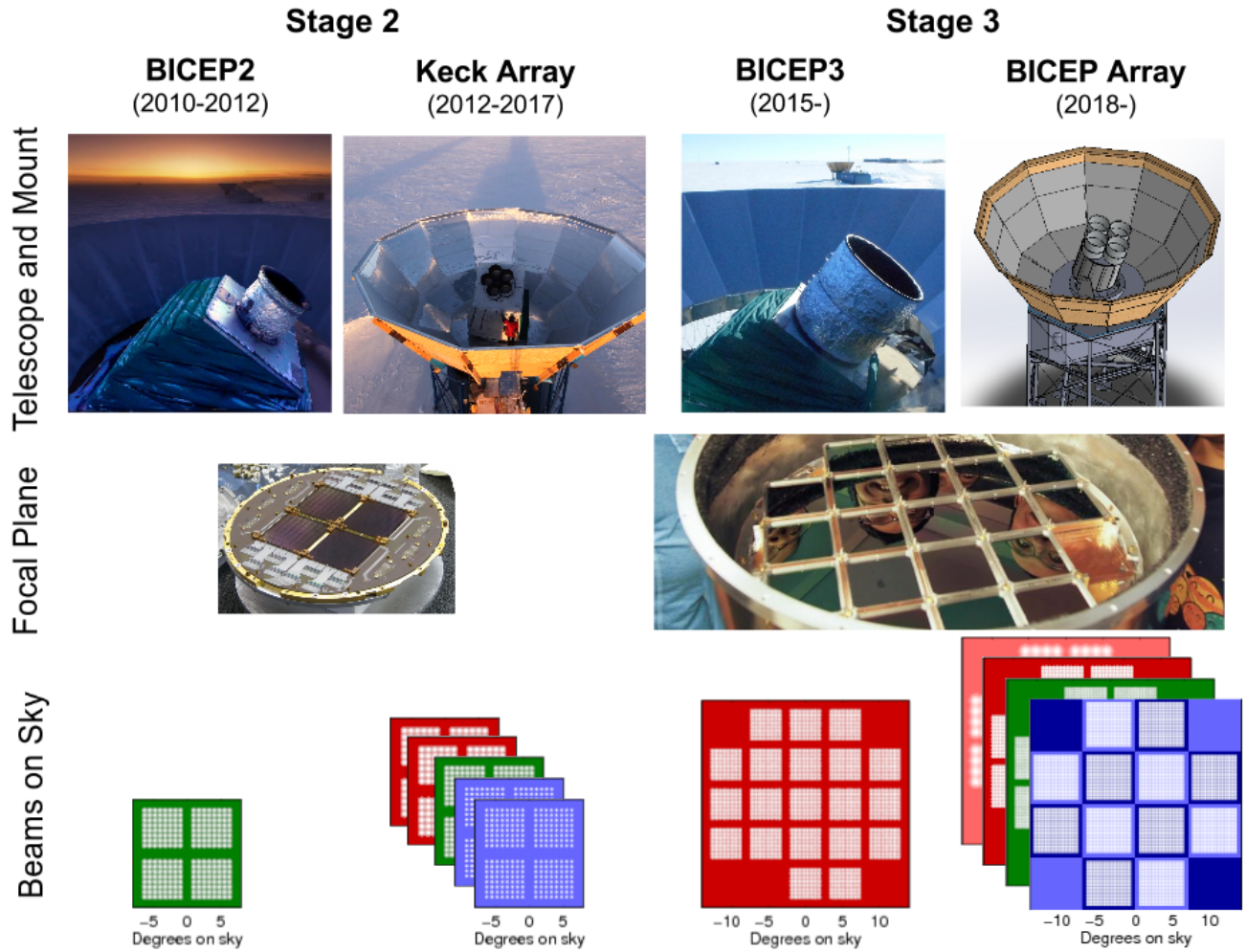


Figure 6: Summary of the 2nd and 3rd-generations of the BICEP/Keck program. The bottom row shows the beam patterns on the sky with a common scale.

It will use a new mount at the existing South Pole *Keck Array* site, and have more than an order of magnitude greater survey weight per receiver versus *Keck Array*.

ACKNOWLEDGMENTS

This work is supported by the National Science Foundation (grant nos. 1313158, 1313010, 1313062, 1313287, 1056465, 0960243), the SLAC Laboratory Directed Research and Development Fund, the Canada Foundation for Innovation, Science and Technology Facilities Council Consolidated Grant (ST/K000926/1), and the British Columbia Development Fund. The development of detector technology was supported by the JPL Research and Technology Development Fund and grants 06-ARPA206-0040, 10-SAT10-0017, and 12-SAT12-0031 from the NASA APRA and SAT programs. The development and testing of detector modules was supported by the Gordon and Betty Moore Foundation.

REFERENCES

- [1] The POLARBEAR Collaboration, Ade, P. A. R., Akiba, Y., Anthony, A. E., Arnold, K., Atlas, M., Barron, D., Boettger, D., Borrill, J., Chapman, S., Chinone, Y., Dobbs, M., Elleflot, T., Errard, J., Fabbian, G., Feng, C., Flanigan, D., Gilbert, A., Grainger, W., Halverson, N. W., Hasegawa, M., Hattori, K., Hazumi, M., Holzzapfel, W. L., Hori, Y., Howard, J., Hyland, P., Inoue, Y., Jaehnig, G. C., Jaffe, A. H., Keating, B., Kermish, Z., Keskitalo, R., Kisner, T., Jeune, M. L., Lee, A. T., Leitch, E. M., Linder, E., Lungu, M., Matsuda, F., Matsumura, T., Meng, X., Miller, N. J., Morii, H., Moyerman, S., Myers, M. J., Navaroli, M., Nishino, H., Orlando, A., Paar, H., Peloton, J., Poletti, D., Quealy, E., Rebeiz, G., Reichardt, C. L., Richards, P. L., Ross, C., Schanning, I., Schenck, D. E., Sherwin, B. D., Shimizu, A., Shimmin, C., Shimon, M., Siritanasak, P., Smecher, G., Spieler, H., Stebor, N., Steinbach, B., Stompor, R., Suzuki, A., Takakura, S., Tomaru, T., Wilson, B., Yadav, A., and Zahn, O., “A Measurement of the Cosmic Microwave Background B-mode Polarization Power Spectrum at Sub-degree Scales with POLARBEAR,” *The Astrophysical Journal* **794**, 171 (October 2014).
- [2] Keisler, R., Hoover, S., Harrington, N., Henning, J. W., Ade, P. A. R., Aird, K. A., Austermann, J. E., Beall, J. A., Bender, A. N., Benson, B. A., Bleem, L. E., Carlstrom, J. E., Chang, C. L., Chiang, H. C., Cho, H.-M., Citron, R., Crawford, T. M., Crites, A. T., de Haan, T., Dobbs, M. A., Everett, W., Gallicchio, J., Gao, J., George, E. M., Gilbert, A., Halverson, N. W., Hanson, D., Hilton, G. C., Holder, G. P., Holzzapfel, W. L., Hou, Z., Hrubes, J. D., Huang, N., Hubmayr, J., Irwin, K. D., Knox, L., Lee, A. T., Leitch, E. M., Li, D., Luong-Van, D., Marrone, D. P., McMahon, J. J., Mehl, J., Meyer, S. S., Mocanu, L., Natoli, T., Nibarger, J. P., Novosad, V., Padin, S., Pryke, C., Reichardt, C. L., Ruhl, J. E., Saliwanchik, B. R., Sayre, J. T., Schaffer, K. K., Shirokoff, E., Smecher, G., Stark, A. A., Story, K. T., Tucker, C., Vanderlinde, K., Vieira, J. D., Wang, G., Whitehorn, N., Yefremenko, V., and Zahn, O., “Measurements of Sub-degree B-mode Polarization in the Cosmic Microwave Background from 100 Square Degrees of SPTpol Data,” *The Astrophysical Journal* **807**, 151 (July 2015).
- [3] BICEP2 Collaboration, Ade, P. A. R., Aikin, R. W., Barkats, D., Benton, S. J., Bischoff, C. A., Bock, J. J., Brevik, J. A., Buder, I., Bullock, E., Dowell, C. D., Duband, L., Filippini, J. P., Fliescher, S., Golwala, S. R., Halpern, M., Hasselfield, M., Hildebrandt, S. R., Hilton, G. C., Hristov, V. V., Irwin, K. D., Karkare, K. S., Kaufman, J. P., Keating, B. G., Kernasovskiy, S. A., Kovac, J. M., Kuo, C. L., Leitch, E. M., Lueker, M., Mason, P., Netterfield, C. B., Nguyen, H. T., O’Brien, R., Ogburn, R. W., Orlando, A., Pryke, C., Reintsema, C. D., Richter, S., Schwarz, R., Sheehy, C. D., Staniszewski, Z. K., Sudiwala, R. V., Teply, G. P., Tolan, J. E., Turner, A. D., Vieregg, A. G., Wong, C. L., and Yoon, K. W., “Detection of B-Mode Polarization at Degree Angular Scales by BICEP2,” *Phys. Rev. Lett.* **112**, 241101 (June 2014).
- [4] Keck Array and BICEP2 Collaborations, Ade, P. A. R., Ahmed, Z., Aikin, R. W., Alexander, K. D., Barkats, D., Benton, S. J., Bischoff, C. A., Bock, J. J., Bowens-Rubin, R., Brevik, J. A., Buder, I., Bullock, E., Buza, V., Connors, J., Crill, B. P., Duband, L., Dvorkin, C., Filippini, J. P., Fliescher, S., Grayson, J., Halpern, M., Harrison, S., Hilton, G. C., Hui, H., Irwin, K. D., Karkare, K. S., Karpel, E., Kaufman, J. P., Keating, B. G., Kefeli, S., Kernasovskiy, S. A., Kovac, J. M., Kuo, C. L., Leitch, E. M., Lueker, M., Megerian, K. G., Netterfield, C. B., Nguyen, H. T., O’Brien, R., Ogburn, R. W., Orlando, A., Pryke, C., Richter, S., Schwarz, R., Sheehy, C. D., Staniszewski, Z. K., Steinbach, B., Sudiwala, R. V., Teply, G. P., Thompson, K. L., Tolan, J. E., Tucker, C., Turner, A. D., Vieregg, A. G., Weber, A. C., Wiebe, D. V., Willmert, J., Wong, C. L., Wu, W. L. K., and Yoon, K. W., “Improved Constraints on Cosmology and Foregrounds from BICEP2 and Keck Array Cosmic Microwave Background Data with Inclusion of 95 GHz Band,” *Phys. Rev. Lett.* **116**, 031302 (January 2016).

- [5] Kamionkowski, M. and Kovetz, E. D., “The Quest for B Modes from Inflationary Gravitational Waves,” *Ann. Rev. Astron. Astrophys.* **54** (September 2016).
- [6] Barkats, D., Aikin, R., Bischoff, C., Buder, I., Kaufman, J. P., Keating, B. G., Kovac, J. M., Su, M., Ade, P. A. R., Battle, J. O., Bierman, E. M., Bock, J. J., Chiang, H. C., Dowell, C. D., Duband, L., Filippini, J., Hivon, E. F., Holzzapfel, W. L., Hristov, V. V., Jones, W. C., Kuo, C. L., Leitch, E. M., Mason, P. V., Matsumura, T., Nguyen, H. T., Ponthieu, N., Pryke, C., Richter, S., Rocha, G., Sheehy, C., Kernasovskiy, S. S., Takahashi, Y. D., Tolan, J. E., and Yoon, K. W., “Degree-scale Cosmic Microwave Background Polarization Measurements from Three Years of BICEP1 Data,” *The Astrophysical Journal* **783**, 67 (March 2014).
- [7] BICEP2/Keck and Planck Collaborations, Ade, P. A. R., Aghanim, N., Ahmed, Z., Aikin, R. W., Alexander, K. D., Arnaud, M., Aumont, J., Baccigalupi, C., Banday, A. J., Barkats, D., Barreiro, R. B., Bartlett, J. G., Bartolo, N., Battaner, E., Benabed, K., Benoît, A., Benoît-Lévy, A., Benton, S. J., Bernard, J.-P., Bersanelli, M., Bielewicz, P., Bischoff, C. A., Bock, J. J., Bonaldi, A., Bonavera, L., Bond, J. R., Borrill, J., Bouchet, F. R., Boulanger, F., Brevik, J. A., Bucher, M., Buder, I., Bullock, E., Burigana, C., Butler, R. C., Buza, V., Calabrese, E., Cardoso, J.-F., Catalano, A., Challinor, A., Chary, R.-R., Chiang, H. C., Christensen, P. R., Colombo, L. P. L., Combet, C., Connors, J., Couchot, F., Coulais, A., Crill, B. P., Curto, A., Cuttaia, F., Danese, L., Davies, R. D., Davis, R. J., de Bernardis, P., de Rosa, A., de Zotti, G., Delabrouille, J., Delouis, J.-M., Désert, F.-X., Dickinson, C., Diego, J. M., Dole, H., Donzelli, S., Doré, O., Douspis, M., Dowell, C. D., Duband, L., Ducout, A., Dunkley, J., Dupac, X., Dvorkin, C., Efstathiou, G., Elsner, F., Enßlin, T. A., Eriksen, H. K., Falgarone, E., Filippini, J. P., Finelli, F., Fliescher, S., Forni, O., Frailis, M., Fraisse, A. A., Franceschi, E., Frejsel, A., Galeotta, S., Galli, S., Ganga, K., Ghosh, T., Giard, M., Gjerløw, E., Golwala, S. R., González-Nuevo, J., Górski, K. M., Gratton, S., Gregorio, A., Gruppuso, A., Gudmundsson, J. E., Halpern, M., Hansen, F. K., Hanson, D., Harrison, D. L., Hasselfield, M., Helou, G., Henrot-Versillé, S., Herranz, D., Hildebrandt, S. R., Hilton, G. C., Hivon, E., Hobson, M., Holmes, W. A., Hovest, W., Hristov, V. V., Hufenberger, K. M., Hui, H., Hurier, G., Irwin, K. D., Jaffe, A. H., Jaffe, T. R., Jewell, J., Jones, W. C., Juvela, M., Karakci, A., Karkare, K. S., Kaufman, J. P., Keating, B. G., Kefeli, S., Keihänen, E., Kernasovskiy, S. A., Kesitalo, R., Kisner, T. S., Kneissl, R., Knoche, J., Knox, L., Kovac, J. M., Krachmalnicoff, N., Kunz, M., Kuo, C. L., Kurki-Suonio, H., Lagache, G., Lähteenmäki, A., Lamarre, J.-M., Lasenby, A., Lattanzi, M., Lawrence, C. R., Leitch, E. M., Leonardi, R., Levrier, F., Lewis, A., Liguori, M., Lilje, P. B., Linden-Vørnle, M., López-Cañiego, M., Lubin, P. M., Lueker, M., Macías-Pérez, J. F., Maffei, B., Maino, D., Mandolesi, N., Mangilli, A., Maris, M., Martin, P. G., Martínez-González, E., Masi, S., Mason, P., Matarrese, S., Megerian, K. G., Meinhold, P. R., Melchiorri, A., Mendes, L., Mennella, A., Migliaccio, M., Mitra, S., Miville-Deschênes, M.-A., Moneti, A., Montier, L., Morgante, G., Mortlock, D., Moss, A., Munshi, D., Murphy, J. A., Naselsky, P., Nati, F., Natoli, P., Netterfield, C. B., Nguyen, H. T., Nørgaard-Nielsen, H. U., Noviello, F., Novikov, D., Novikov, I., O’Brien, R., Ogburn, R. W., Orlando, A., Pagano, L., Pajot, F., Paladini, R., Paoletti, D., Partridge, B., Pasian, F., Patanchon, G., Pearson, T. J., Perdereau, O., Perotto, L., Pettorino, V., Piacentini, F., Piat, M., Pietrobon, D., Plaszczynski, S., Pointecouteau, E., Polenta, G., Ponthieu, N., Pratt, G. W., Prunet, S., Pryke, C., Puget, J.-L., Rachen, J. P., Reach, W. T., Rebolo, R., Reinecke, M., Remazeilles, M., Renault, C., Renzi, A., Richter, S., Ristorcelli, I., Rocha, G., Rossetti, M., Roudier, G., Rowan-Robinson, M., Rubiño Martín, J. A., Rusholme, B., Sandri, M., Santos, D., Savelainen, M., Savini, G., Schwarz, R., Scott, D., Seiffert, M. D., Sheehy, C. D., Spencer, L. D., Staniszewski, Z. K., Stolyarov, V., Sudiwala, R., Sunyaev, R., Sutton, D., Suur-Uski, A.-S., Sygnet, J.-F., Tauber, J. A., Tephy, G. P., Terenzi, L., Thompson, K. L., Toffolatti, L., Tolan, J. E., Tomasi, M., Tristram, M., Tucci, M., Turner, A. D., Valenziano, L., Valiviita, J., Van Tent, B., Vibert, L., Vielva, P., Vieregg, A. G., Villa, F., Wade, L. A., Wandelt, B. D., Watson, R., Weber, A. C., Wehus, I. K., White, M., White, S. D. M., Willmert, J., Wong, C. L., Yoon, K. W., Yvon, D., Zacchei, A., and Zonca, A., “Joint Analysis of BICEP2/ *Keck Array* and *Planck* Data,” *Phys. Rev. Lett.* **114**, 101301 (March 2015).
- [8] Ahmed, Z., Amiri, M., Benton, S. J., Bock, J. J., Bowens-Rubin, R., Buder, I., Bullock, E., Connors, J., Filippini, J. P., Grayson, J. A., Halpern, M., Hilton, G. C., Hristov, V. V., Hui, H., Irwin, K. D., Kang, J., Karkare, K. S., Karpel, E., Kovac, J. M., Kuo, C. L., Netterfield, C. B., Nguyen, H. T., O’Brien, R., Ogburn, R. W., Pryke, C., Reintsema, C. D., Richter, S., Thompson, K. L., Turner, A. D., Vieregg, A. G., Wu, W. L. K., and Yoon, K. W., “BICEP3: a 95 GHz refracting telescope for degree-scale CMB

polarization,” in [*Millimeter, Submillimeter, and Far-Infrared Detectors and Instrumentation for Astronomy VII*], *Proc. SPIE* **9153**, 91531N (August 2014).

- [9] Wu, W. L. K., *BICEP3 and CMB-S4: current and future CMB polarization experiments to probe fundamental physics*, PhD thesis, Stanford University (2015).
- [10] Ade, P. A. R., Aikin, R. W., Amiri, M., Barkats, D., Benton, S. J., Bischoff, C. A., Bock, J. J., Bonetti, J. A., Brevik, J. A., Buder, I., Bullock, E., Chattopadhyay, G., Davis, G., Day, P. K., Dowell, C. D., Duband, L., Filippini, J. P., Fliescher, S., Golwala, S. R., Halpern, M., Hasselfield, M., Hildebrandt, S. R., Hilton, G. C., Hristov, V., Hui, H., Irwin, K. D., Jones, W. C., Karkare, K. S., Kaufman, J. P., Keating, B. G., Kefeli, S., Kernasovskiy, S. A., Kovac, J. M., Kuo, C. L., LeDuc, H. G., Leitch, E. M., Llobart, N., Lueker, M., Mason, P., Megerian, K., Moncelsi, L., Netterfield, C. B., Nguyen, H. T., O’Brien, R., IV, R. W. O., Orlando, A., Pryke, C., Rahlin, A. S., Reintsema, C. D., Richter, S., Runyan, M. C., Schwarz, R., Sheehy, C. D., Staniszewski, Z. K., Sudiwala, R. V., Tephy, G. P., Tolan, J. E., Trangsrud, A., Tucker, R. S., Turner, A. D., Vieregg, A. G., Weber, A., Wiebe, D. V., Wilson, P., Wong, C. L., Yoon, K. W., Zmuidzinas, J., and for the BICEP2, Keck Array, and Spider Collaborations, “Antenna-coupled TES Bolometers Used in BICEP2, Keck Array, and Spider,” *The Astrophysical Journal* **812**, 176 (October 2015).
- [11] O’Brien, R., Ade, P. A. R., Ahmed, Z., Aikin, R. W., Amiri, M., Benton, S., Bischoff, C., Bock, J. J., Bonetti, J. A., Brevik, J. A., Burger, B., Davis, G., Day, P., Dowell, C. D., Duband, L., Filippini, J. P., Fliescher, S., Golwala, S. R., Grayson, J., Halpern, M., Hasselfield, M., Hilton, G., Hristov, V. V., Hui, H., Irwin, K., Kernasovskiy, S., Kovac, J. M., Kuo, C. L., Leitch, E., Lueker, M., Megerian, K., Moncelsi, L., Netterfield, C. B., Nguyen, H. T., Ogburn, R. W., Pryke, C. L., Reintsema, C., Ruhl, J. E., Runyan, M. C., Schwarz, R., Sheehy, C. D., Staniszewski, Z., Sudiwala, R., Tephy, G., Tolan, J. E., Turner, A. D., Tucker, R. S., Vieregg, A., Wiebe, D. V., Wilson, P., Wong, C. L., Wu, W. L. K., and Yoon, K. W., “Antenna-coupled TES bolometers for the Keck array, Spider, and Polar-1,” in [*Millimeter, Submillimeter, and Far-Infrared Detectors and Instrumentation for Astronomy VI*], *Proc. SPIE* **8452**, 84521G (September 2012).
- [12] Hui, H. et al., “Second year detectors performance of BICEP3,” in [*these proceedings*], *Proc. SPIE* (2016).
- [13] de Korte, P. A. J., Beyer, J., Deiker, S., Hilton, G. C., Irwin, K. D., MacIntosh, M., Nam, S. W., Reintsema, C. D., Vale, L. R., and Huber, M. E., “Time-division superconducting quantum interference device multiplexer for transition-edge sensors,” *Review of Scientific Instruments* **74**(8), 3807–3815 (2003).
- [14] Battistelli, E. S., Amiri, M., Burger, B., Halpern, M., Knotek, S., Ellis, M., Gao, X., Kelly, D., Macintosh, M., Irwin, K., and Reintsema, C., “Functional Description of Read-out Electronics for Time-Domain Multiplexed Bolometers for Millimeter and Sub-millimeter Astronomy,” *Journal of Low Temperature Physics* **151**, 908–914 (May 2008).
- [15] Ahmed, Z., Grayson, J. A., Thompson, K. L., Kuo, C.-L., Brooks, G., and Pothoven, T., “Large-Area Reflective Infrared Filters for Millimeter/Sub-mm Telescopes,” *Journal of Low Temperature Physics* **176**(5), 835–840 (2014).
- [16] Ade, P. A. R., Pisano, G., Tucker, C., and Weaver, S., “A review of metal mesh filters,” *Proc. SPIE* **6275**, 62750U–62750U–15 (2006).
- [17] Wu, W. L. K., Ade, P. A. R., Ahmed, Z., Alexander, K. D., Amiri, M., Barkats, D., Benton, S. J., Bischoff, C. A., Bock, J. J., Bowens-Rubin, R., Buder, I., Bullock, E., Buza, V., Connors, J. A., Filippini, J. P., Fliescher, S., Grayson, J. A., Halpern, M., Harrison, S., Hilton, G. C., Hristov, V. V., Hui, H., Irwin, K. D., Kang, J., Karkare, K. S., Karpel, E., Kefeli, S., Kernasovskiy, S. A., Kovac, J. M., Kuo, C. L., Megerian, K. G., Netterfield, C. B., Nguyen, H. T., O’Brien, R., Ogburn, R. W., Pryke, C., Reintsema, C. D., Richter, S., Sorensen, C., Staniszewski, Z. K., Steinbach, B., Sudiwala, R. V., Tephy, G. P., Thompson, K. L., Tolan, J. E., Tucker, C. E., Turner, A. D., Vieregg, A. G., Weber, A. C., Wiebe, D. V., Willmert, J., and Yoon, K. W., “Initial Performance of BICEP3: A Degree Angular Scale 95 GHz Band Polarimeter,” *Journal of Low Temperature Physics* (December 2015).
- [18] Karkare, K. S., Ade, P. A. R., Ahmed, Z., Aikin, R. W., Alexander, K. D., Amiri, M., Barkats, D., Benton, S. J., Bischoff, C. A., Bock, J. J., Bonetti, J. A., Brevik, J. A., Buder, I., Bullock, E. W., Burger, B., Connors, J., Crill, B. P., Davis, G., Dowell, C. D., Duband, L., Filippini, J. P., Fliescher, S. T., Golwala, S. R., Gordon, M. S., Grayson, J. A., Halpern, M., Hasselfield, M., Hildebrandt, S. R., Hilton, G. C., Hristov, V. V., Hui, H., Irwin, K. D., Kang, J. H., Karpel, E., Kefeli, S., Kernasovskiy, S. A., Kovac, J. M., Kuo,

C. L., Leitch, E. M., Lueker, M., Mason, P., Megerian, K. G., Netterfield, C. B., Nguyen, H. T., O'Brien, R., Ogburn, R. W., Pryke, C. L., Reintsema, C. D., Richter, S., Schwarz, R., Sheehy, C. D., Staniszewski, Z. K., Sudiwala, R. V., Teply, G. P., Thompson, K. L., Tolan, J. E., Turner, A. D., Viereg, A., Weber, A., Wong, C. L., Wu, W. L. K., and Yoon, K. W., "Keck array and BICEP3: spectral characterization of 5000+ detectors," in [*Millimeter, Submillimeter, and Far-Infrared Detectors and Instrumentation for Astronomy VII*], *Proc. SPIE* **9153**, 91533B–91533B–11 (August 2014).

- [19] Karkare, K. S. et al., "Optical characterization of the BICEP3 CMB polarimeter at the South Pole," in [*these proceedings*], *Proc. SPIE* (2016).